Heterogeneous & Homogeneous & Bio- & Nano-
CHEMCATCHEM
CATALYSIS

Accepted Article

Title: Understanding the role of SnO2 support in water-tolerant methane combustion: In situ observation of Pd(OH)2 and comparison with Pd/Al2O3

Authors: William Barrett, Jing Shen, Yongfeng Hu, Robert E. Hayes, Robert W.J. Scott, and Natalia Semagina

To be cited as: *ChemCatChem* 10.1002/cctc.201901744

Link to VoR: http://dx.doi.org/10.1002/cctc.201901744

A Journal of ChemPubSoc Europe

WILEY-VCH www.chemcatchem.org

ChemCatChem

10.1002/cctc.201901744

WILEY-VCH

FULL PAPER

Understanding the role of SnO_2 support in water-tolerant methane combustion: *In situ* observation of $Pd(OH)_2$ and comparison with Pd/Al_2O_3

William Barrett,[#][b] Jing Shen,[#][a] Yongfeng Hu,[c] Robert E. Hayes,[a] Robert W.J. Scott,*[b] and Natalia Semagina*[a]

Abstract: Quantitative analysis of poisonous Pd hydroxide phase formation during methane combustion in the presence of water is performed via *in situ* X-ray absorption spectroscopy from 200 to 500 deg C for palladium catalysts supported on tin and aluminum oxides. Water presence inhibits oxidation of the metallic Pd; for the Pd/Al_2O_3 catalyst the major oxidation product is $Pd(OH)_2$, with PdO being the dominant phase on the Pd/SnO_2 system. Tin dioxide is reduced during methane oxidation in the presence of water, regardless of the excess oxygen in the feed. Temperature-programmed surface reactions at anaerobic and low-oxygen conditions revealed that the Pd/SnO_2 catalyst has an inability to catalyze methane steam reforming, as opposed to Pd/Al_2O_3. We suggest that tin oxide extracts hydroxyls from the PdO surface, which makes the latter more active in methane combustion in the presence of water but inactive in methane steam reforming.

Introduction

One of the major requirements of an efficient catalyst for exhaust aftertreatment from lean-burn natural gas vehicles is its water tolerance at low operating temperatures (below 500 °C). Conventional Pd/Al_2O_3 catalysts are known for their instability at such conditions due to the water and hydroxyl accumulation on the active sites and/or support. [1] Deactivation of PdO active sites is accepted to occur via the formation of inactive $Pd(OH)_2$ at temperatures below 450 °C (for Pd/Al_2O_3).[2,3] Pfefferle and colleagues advocated that water impedes oxygen mobility on the support, thus, its detrimental effect may be balanced by the use of a support with high oxygen mobility,[4–7] which was corroborated by other groups for the supports with high oxygen-storage capacity[8] or hydrophobicity.[3] Our earlier *in situ* X-ray absorption spectroscopy study provided evidence of the lack of oxygen at Pd active sites in the wet feed at low temperatures in Pd/Al_2O_3 system,[9] which was supported by others.[10]

Among a myriad of reported catalysts, SnO_2-supported Pt-group materials have a rather extraordinary resistance to water poisoning in wet methane combustion.[11,12] We have previously shown (Figure 1[13]) that Pd/SnO_2 can surpass even $Pd\text{-}Pt/Al_2O_3$ in its activity in the presence of water; studies by others[11] and ourselves[13] also report insignificant variations in methane conversion when the water content in the feed was increased up to 20%. A kinetic study[11] revealed a more negative enthalpy of H_2O adsorption on Pd/Al_2O_3 than on Pd/SnO_2, which was suggested as a reason of high water tolerance of the latter system. The SnO_2 reducibility was also noted as an important contributor to the Pd/SnO_2 activity because of hypothesized lattice oxygen spillover, although in the absence of added water. [14]

Our selective attention to Pd/SnO_2 was also fuelled by the fact that SnO_2 is used as sensors for CO and (less frequently) CH_4 or H_2 detection via catalytic oxidation mechanisms.[15–32] The humidity effect has been known in that field since 1970's[16–18,24–32] as it influences the sensor signal by electron generation: $H_2O + Sn_{lattice} + O_{lattice} \Leftrightarrow (HO\text{-}Sn_{lattice}) + (O_{lattice}H)^+ + e^-$.[19] SnO_x surface has a high affinity to water that competes with CO adsorption;[27]

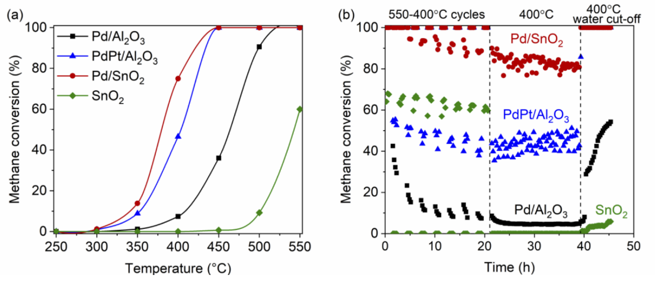

Figure 1. (a) Ignition tests of methane combustion in the presence of 5% water; and (b) hydrothermal ageing test (the temperature was varied between 400 and 500 °C, after which it was held constant). The tests are done at the same total Pd loading in the reactor. Metal dispersion in Pd/SnO_2, Pd/Al_2O_3 and $PdPt/Al_2O_3$ catalysts is 11%, 43% and 10%, respectively. Reprinted from [13] by permission from Springer Nature, Copyright 2018.

---

[a] Prof. N. Semagina, Dr. J. Shen, Prof. R.E. Hayes
Department of Chemical and Materials Engineering
University of Alberta, 9211-116 St. Edmonton AB T6G 1H9, Canada
E-mail: semagina@ualberta.ca
[b] Prof. R.W.J. Scott, W. Barrett
Department of Chemistry, University of Saskatchewan
110 Science Place, Saskatoon SK S7N 5C9 Canada
E-mail: robert.scott@usask.ca
[c] Dr. Y. Hu
Canadian Light Source Inc.
44 Innovation Boulevard, Saskatoon SK S7N 2V3 Canada

# co-first authors, contributed equally

Supporting information for this article can be found on-line.

the concentration of hydroxyl groups increases in the presence of gas-phase water and O_2.[20] In H_2 sensing, in the presence of O_2, water formation occurs as expected, while at anaerobic conditions, hydrogen reacts with the metal oxide surface to create "rooted" hydroxyl groups and there is no detected desorbed water formation.[21] In Pd/SnO_2 systems, CO activated on PdO_x reacts with hydroxyls on SnO_2 surface with CO_2 formation.[23] CH_x reaction intermediates on Pt-group active sites can be oxidized by OH_{ads} on adjacent oxophilic Sn surface.[33]

In this work we follow the Pd speciation by X-ray absorption spectroscopy (XAS) of Pd/Al_2O_3 and Pd/SnO_2 catalysts during methane combustion in the wet feed to observe the presence of $Pd(OH)_2$ hydroxyl species on Pd/PdO particles and to understand better the influence of the support on the water tolerance. Typically, hydroxyl formation in methane combustion has been determined by operando or *in situ* infrared spectroscopy; however that does not typically allow one to distinguish hydroxyl groups presents on the Pd and the support surface.[3,4,8] Herein, we were able to track the metallic Pd, PdO and $Pd(OH)_2$ via *in situ* Pd L edge and K edge XAS studies at temperatures applicable to lean-burn methane combustion in the presence of water. The XAS data are complemented by reactions at different O_2/CH_4 in the feed (0 through 1.9 mol/mol) that also demonstrate a strikingly unusual and unexpected feature of the Pd/SnO_2 catalyst as compared to Pd/Al_2O_3 with respect to water activation.

Results and Discussion

In situ X-ray absorption study (XAS): pretreatment and selection of standards

When a PdO catalyst is exposed to methane combustion in the wet feed, it progressively becomes reduced, as observed by Monaie *et al.* [8] via *in situ* X-ray absorption spectroscopy over 80 min on stream at 600 °C, while PdO remained oxidized with no water addition to the feed. The rather slow phenomenon is in line with the Pd/Al_2O_3 deactivation profile from Figure 1b. Our earlier *in situ* XAS study of the reduced Pd/Al_2O_3 catalyst in lean-fuel methane combustion without added water in the feed demonstrated that the metallic Pd was completely oxidized by the start of the catalytic test (200 °C).[9] In the presence of water in the feed, the Pd(0) fraction remained dominant up to *about* 350 °C,[9] which confirmed the earlier hypothesis of Pfefferle and colleagues that water inhibits oxygen migration and exchange.[7] PdO is accepted as a more active phase than metallic Pd in methane combustion,[8,34] or it is at least required in pair with Pd(0) for C-H activation.[35] Since the presence of water and nature of the support were suggested to influence the onset and the rate of Pd(0) reoxidation process,[5] we reduced the studied calcined PdO/Al_2O_3 and PdO/SnO_2 catalysts prior to the *in situ* XAS analysis.

Figure 2 shows temperature-programmed reduction (TPR) profiles of the catalysts and the pure SnO_2 support. Bulk SnO_2 reduction is known to occur above 500 °C,[36,37] while the lower-temperature peaks (α, β and γ) can be assigned to the reduction of surface adsorbed oxygen species, lattice oxygen on SnO_2 surface, and amorphous SnO_2, respectively [29]. Alternatively, the low temperature shoulder reduction peaks of SnO_2 at low temperatures were attributed to the reduction of surface adsorbed oxygen and Sn^{4+} to Sn^{2+}.[38] Pd addition to SnO_2 expectedly shifts the reduction onset to lower temperatures due to hydrogen spillover from reduced Pd. The low-temperature PdO reduction, Pd hydride formation and decomposition occurs on both Pd/Al_2O_3 and Pd/SnO_2 catalysts. Thus, to exclude the effect of labile support oxygen on the speciation during in situ methane combustion, we prereduced both catalysts at 300 °C.

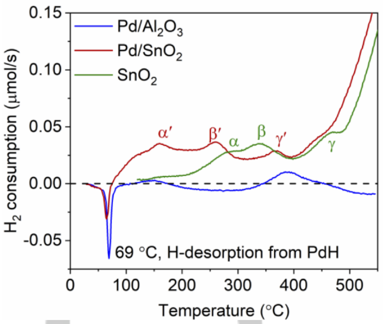

Figure 2. TPR profiles of SnO_2, Pd/SnO_2 and Pd/Al_2O_3 (0.5 g each). Heating rate is 10 °C/min. H_2 consumption was monitored by a calibrated on-line mass spectrometer.

Figure S1 in the Supporting Information presents XPS profiles of the Pearlman's catalyst $Pd(OH)_2/C$ and fresh (calcined) Pd/SnO_2 that served as $Pd(OH)_2$ and PdO standards for the *in situ* XAS studies. The Pearlman's catalyst is characterized by Albers et al.,[39] so the $3d_{5/2}$ peak at ~337.5 eV can be assigned to $Pd(OH)_2$. As expected after the calcination, the Pd/SnO_2 sample is primarily PdO (~336.3 eV; 89%) with contributions from Pd (~335.3 eV; 5%), and $Pd(OH)_2$ (~337.5 eV) 6%. The palladium metal is created via the reduction of PdO by X-rays under vacuum, suggesting the concentration of PdO on the surface could be up to 94%.

In situ XAS: Pd speciation during methane combustion in the wet feed

In the current spectroscopic study of the water effect during in situ methane combustion, we use Pd K (and complement with Pd L edge data) to differentiate the evolution of Pd(0), PdO, and $Pd(OH)_2$ species with temperature. The Pd K edge is primarily transitions from 1s to 4p and, therefore, is sensitive to speciation and relatively insensitive to species interacting with the surface (primarily 4d interactions). Note that the XANES region is not significantly temperature sensitive, which allows for linear combination fitting of the data over multiple temperatures. Due to conformational and oxidation state differences between the materials we were able to distinguish between species via the XANES portion of the XAS data. *In situ* Pd K edge data for the Pd/SnO_2 catalyst in wet conditions are shown in Figure 3, along with the reference spectra used for linear combination fitting. Figure 3a presents changes in the Pd/SnO_2 spectra as a function

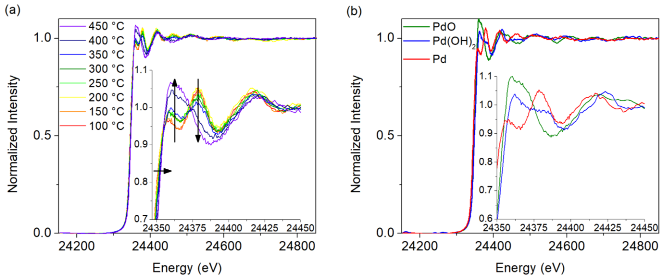

Figure 3. Pd K edge XAS spectra of Pd/SnO$_2$ (a) under *in situ* wet methane oxidation conditions, and (b) Pd standards.

of temperature and the inset highlights the XANES region. Two trends are obvious, as shown by vertical and horizontal arrows. The horizontal arrows indicate the white line is shifting to higher energy, while the vertical arrows show the growth in the feature at about 24360 eV and loss of the feature at about 24380 eV. These changes are consistent with Pd oxidation as can be seen by comparing with Pd(0), PdO and Pd(OH)$_2$ reference spectra in Figure 3b. There are no major changes in spectra at low temperatures (100 °C – 200 °C), followed by slow oxidation at moderate temperatures (200 °C - 350 °C) and nearly complete oxidation at higher temperatures (400 °C - 450 °C). The spectra of the Pd/SnO$_2$ sample heated at 450 °C under methane oxidation conditions closely resembles the spectra of the PdO standard. Previously obtained *in situ* data of the K-edge of Pd/Al$_2$O$_3$[9] shows a similar trend consistent with Pd oxidation at higher temperatures.

Figure 4 shows the Pd L$_3$ edge data for Pd on both SnO$_2$ and Al$_2$O$_3$ supports. The white line at the L$_3$ edge of Pd probes the $2p_{3/2}$ to 4d transition, and thus the occupancy of the valence 4d band of Pd, and therefore is sensitive to both Pd speciation, and to intermediates interacting with the Pd surface. Figure 4a shows that from 100 °C – 200 °C, the original white line broadens slightly and the peak maxima is relatively static. At moderate temperatures, the spectra shift to slightly higher energies, with a slight increase in the white line intensity. Finally, beyond 350 °C the white line shifts slightly to lower energy and increases slightly in intensity. On comparison with Pd standards in Figure 4c, this suggests mild oxidation of the samples at higher temperature, which is consistent with K edge data, although the Pd L$_3$ edge data suggests a lesser degree of Pd oxidation. One possible rationale for the differences seen in the Pd L$_3$ and K edge data for Pd/SnO$_2$ samples is that for lower energy L$_3$ edge studies, the gaseous environment needed to be switched to He during measurements to prevent X-ray scattering of the gaseous atmosphere, whereas for K edge measurements, this change in atmosphere was not necessary. It is possible that some Pd photoreduction may occur while under the He atmosphere.

Pd L$_3$ edge data for the Pd/Al$_2$O$_3$ sample are shown in Figure 4b. As the temperature increases, the white line drifts right and increases significantly in intensity, indicative of a fast oxidation of the sample and consistent with major Pd speciation changes. As noted in Figure 4c, the measured white line intensity of Pd(OH)$_2$ standards is much higher than that seen for PdO, which suggests the Pd in Pd(OH)$_2$ is more 4d electron deficient. Thus the Pd/Al$_2$O$_3$ data suggests that significant Pd(OH)$_2$ is formed in the Al$_2$O$_3$ system that is absent in the SnO$_2$ system. We do note that at 400 °C the intensity of the white line of the Pd/Al$_2$O$_3$ sample is above even that of the Pd(OH)$_2$ standard, which suggests that another 4d-electron withdrawing species is present on the surface. This may be due to the presence of formate groups on the surface, as others have shown that formate species can be long living intermediates in the methane combustion pathway.[40]

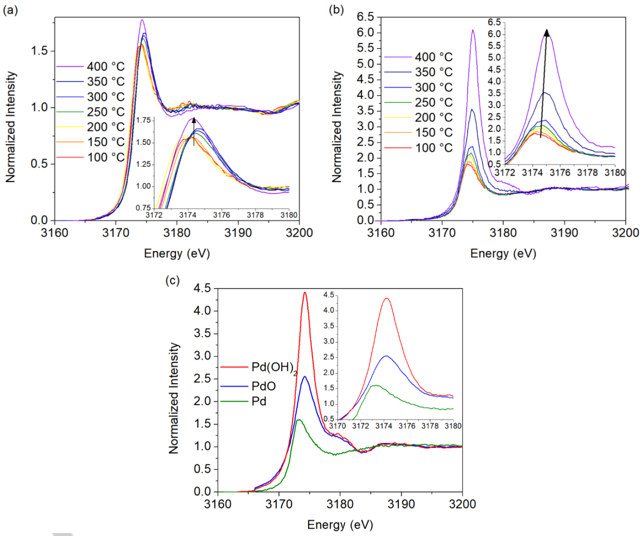

Figure 4. Pd L$_3$ edge XAS spectra of (a) Pd/SnO$_2$ and (b) Pd/Al$_2$O$_3$ under *in situ* wet methane oxidation conditions, and (c) Pd standards.

Figure 5 presents the LCF fitting of the Pd K edge for both Pd/SnO$_2$ and Pd/Al$_2$O$_3$ samples. Data used for the Pd/Al$_2$O$_3$ data is from our previous study, which used similar catalysts studied under similar reaction conditions.[9] LCF was not done with Pd L$_3$ edge data, given the possibility that surface speciation and/or photoreduction changes may be influencing the spectra in the Pd L$_3$ edge. The Pd/SnO$_2$ catalyst data in Figure 5a shows that Pd metal slowly oxidizes with the formation of both PdO as a dominant oxidation product and Pd(OH)$_2$ as a minor product. At higher temperatures, a complete dehydration of Pd(OH)$_2$ is seen, which is consistent with the dehydration onset suggested in the literature based on kinetic studies.[2,3] The maximum observed Pd(OH)$_2$ fraction on Pd/SnO$_2$ of 15% at 350 °C closely resembles the Pd surface area of the catalyst (16% metal dispersion as determined by CO chemisorption). This suggests coexistence and competition between PdO and Pd(OH)$_2$ for the surface area below 350 °C. Earlier transient studies also showed that in that temperature region the water effect has not reached equilibrium.[1]

For the Pd/Al$_2$O$_3$ system with 40% Pd dispersion, as Figure 5b demonstrates, Pd(OH)$_2$ is the only observed Pd(0) oxidation product up to 350 °C, when PdO also appears. This marks the onset of catalytic activity (Figure 1), that occurs at higher temperature as compared to Pd/SnO$_2$ system where PdO exists already at 100 °C.

Indeed, PdO is accepted as a more active phase than metallic Pd in methane combustion.[8,34,41,42] One should keep in mind, however, that the Pd (re)-oxidation is kinetically limited, and both the kinetics and thermodynamics are particle-size dependent.[41,43,44] A recent operando XAS study of Pd/Al_2O_3 catalysts with monodispersed Pd particles (3-16 nm range) in wet methane combustion[41] confirmed that at least partially oxidized surface is required for methane combustion. Our study lacks the size uniformity of the Pd particles, but the starting Pd colloidal solution contains 2-nm Pd particles, which sinter to larger particles with 40% dispersion on Al_2O_3 and 16% on SnO_2 with a lower surface area. It cannot be excluded that the higher achieved degree of Pd hydroxylation on Al_2O_3 (up to 70%) is due to the smaller Pd particle size. However, at temperatures below 300 °C (Figure 5), both Pd/Al_2O_3 and Pd/SnO_2 catalysts are oxidized to the same extent of approximately 25%, which is insignificantly below the Pd dispersion on Al_2O_3 or above the dispersion on SnO_2. Dramatic changes in the Pd speciation happen around the Pd dispersion values (within 10-15%, which may account for the particle polydispersity). For such surface/near-sub-surface oxidation, the two catalysts are distinctly different: $Pd(OH)_2$ dominates the surface of Pd/Al_2O_3 catalyst, before even the appearance of PdO, while PdO is prevalent on the Pd/SnO_2 surface before the appearance of $Pd(OH)_2$. Thus, the support dramatically alters the observed speciation of oxidized Pd species and affects the catalytic behavior.

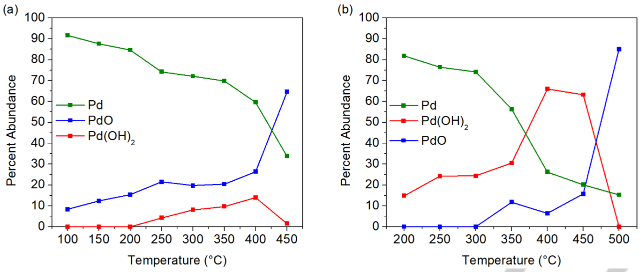

Figure 5. LCF of Pd K edge XAS data for Pd/SnO_2 and (b) Pd/Al_2O_3 under *in situ* wet methane oxidation conditions. Pd dispersion is 16% for Pd/SnO_2 and 40% for Pd/Al_2O_3.

In situ XAS: Sn L_3 edge during wet methane combustion

The Sn L_3 edge is presented in Figure 6. Due to the larger particle size of the SnO_2 support (44 μm) the fitting of this species is significantly easier, however, is less sensitive. This is because the surface, the most active and complex part of a fit, is not a substantial percentage of the SnO_2 particles and therefore, the technique is not significantly sensitive to the surface speciation. Commercial SnO and SnO_2 were used as standards and the overlay indicates SnO_2 to SnO conversion between 100 °C and 250 °C above which the system is relatively stable. The *in situ* analysis of Sn L-edge (Figure 6) demonstrates approximately 10% reduction of SnO_2 to SnO at 100 °C, as expected from the catalyst pretreatment, which increased to 30% at 250 °C and stabilized up to 400 °C. The reduction could occur by electrons liberated during SnO_2 hydroxylation as $H_2O + Sn_{lattice} + O_{lattice} \Leftrightarrow (HO\text{-}Sn_{lattice}) + (O_{lattice}H)^+ + e^-$. [27] Note that this reduction occurs *in situ* at excess oxygen in the feed.

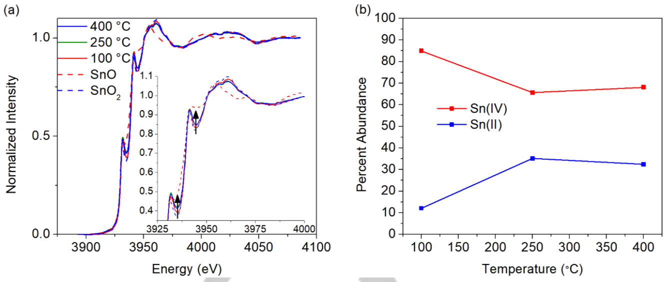

Figure 6. Sn L_3 edge XAS data for (a) Pd/SnO_2 and (b) LCF fit of data using SnO and SnO_2 standards.

Oxygen and water effects on the Pd/SnO_2 and Pd/Al_2O_3 catalysts

Figure 5 shows an expected trend of Pd(0) decrease with the temperature increase, and the metal oxidation rate is suppressed by the presence of water.[7,9,10] However, the SnO_2/SnO support promotes the formation of PdO, while mostly $Pd(OH)_2$ is observed on the Al_2O_3 support. To evaluate the metal oxide interaction with water, we calculated standard Gibbs free energies of endothermic dehydroxylation reactions R(1)-R(3) at 300 °C. Constant heats of reaction and validity of short-cut van't Hoff's equation were assumed; the thermodynamic properties at 298.15 K for $Al(OH)_3$ are from [45], for $Sn(OH)_2$ are from [46], for $Pd(OH)_2$ are from [47,48].

R1). $2/3\ Al(OH)_3 \rightleftharpoons 1/3\ Al_2O_3 + H_2O$ $\Delta G^{o}_{573K} = -36\ kJ/mol_{H_2O}$
R2). $Pd(OH)_2 \rightleftharpoons PdO + H_2O$ $\Delta G^{o}_{573K} = -25\ kJ/mol_{H_2O}$
R3). $Sn(OH)_2 \rightleftharpoons SnO + H_2O$ $\Delta G^{o}_{573K} = -19\ kJ/mol_{H_2O}$

The dehydroxylation trend indicates that the hydroxylated inactive $Pd(OH)_2$ may coexist with dehydroxylated Al_2O_3, while in the Pd/SnO_2 system SnO can potentially serve as a sink for water released from $Pd(OH)_2$, followed by $Sn(OH)_2$ dehydroxylation, which potentially can explain the speciation observed in Figure 5.

To further clarify the oxygen and water effect on methane conversion for the two catalysts, we performed a series of experiments with various substoichiometric O_2/CH_4 ratios (0 – 1.9 mol/mol) and monitored evolved species by an on-line mass spectrometer calibrated for CH_4, O_2, H_2O, CO_2, CO and H_2. As seen from Figures 7a and 7c, upon the O_2 exhaustion in the feed, the Pd/Al_2O_3 catalyst was able to continue methane conversion in the presence of CO_2 and H_2O. The nearly constant CO_2 concentration and increasing CO and H_2 concentration at the expense of H_2O and CH_4 are characteristics of methane steam reforming, as expected for Pd/Al_2O_3 catalyst.[49] The Pd/SnO_2 catalyst shows a strikingly unusual behavior (Figures 7b and 7d). Upon complete oxygen consumption, no methane conversion was observed for any of the tested O_2/CH_4 ratios. The mixture of CH_4, H_2O, CO_2 and minor CO remained unreactive at temperatures between 400 and 550 °C, where normally Pd is expected to catalyze the methane steam reforming. Although Pd poisoning by thin tin oxide shell may occur,[24,50,51] this could not explain the observed behavior because every presented ignition

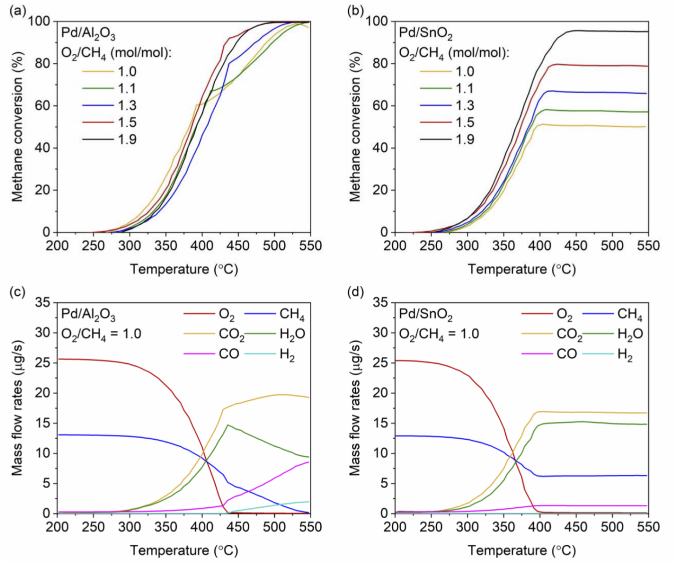

Figure 7. Ignition curves (a,b) for CH_4 combustion at constant O_2 and variable CH4 (5000 – 9000 ppm) concentrations, and (c, d) product distribution for O_2/CH_4 ratio of 1.0 mol/mol on Pd/Al_2O_3 and Pd/SnO_2 catalysts. 10 °C/min heating rate. See Table 1 for other reaction conditions.

curve was measured five times in each set, and two sets of experiments were performed in variable methane concentration order; all tests systematically show less than 3% conversion deviation. The blocking film cannot appear above 400 °C and disappear at lower temperatures every time at multiple cycling while producing highly repeatable kinetic curves. The only possible scenario for the observed behavior is that the Pd/SnO_2 catalyst is not able to activate H_2O for methane steam reforming (and we know that CH_4 activation on Pd is possible because of the successful combustion while O_2 supplies lasted, Figure 7c).

This property would explain the catalyst tolerance to water for the wet methane combustion (Figures 1 and 5b). Apparently, SnO_2 indeed extracts hydroxyls from PdO, which Al_2O_3 was not able to achieve, which was seen by the *in situ* XAS (Figure 5). In Pd/Al_2O_3 catalyst after the feed oxygen exhaustion $Pd(OH)_2$ and activated CH_4*-Pd can coexist on Pd surface and lead to methane steam reforming, while in Pd/SnO_2 system the hydroxyls were formed on the tin surface instead of Pd and could not participate in the reforming reaction.

There is also a hypothesis in the literature that tin oxide may provide its lattice oxygen to Pd.[14] However, Figure 7d shows that the minor amount of CO (formed while molecular O_2 supplies lasted) was not converted to CO_2 when no O_2 was present in the feed. To further clarify the possible oxygen donation from SnO_2 to Pd, we performed temperature-programmed surface reactions (TPSRs) with methane at anaerobic conditions (Figure 8).

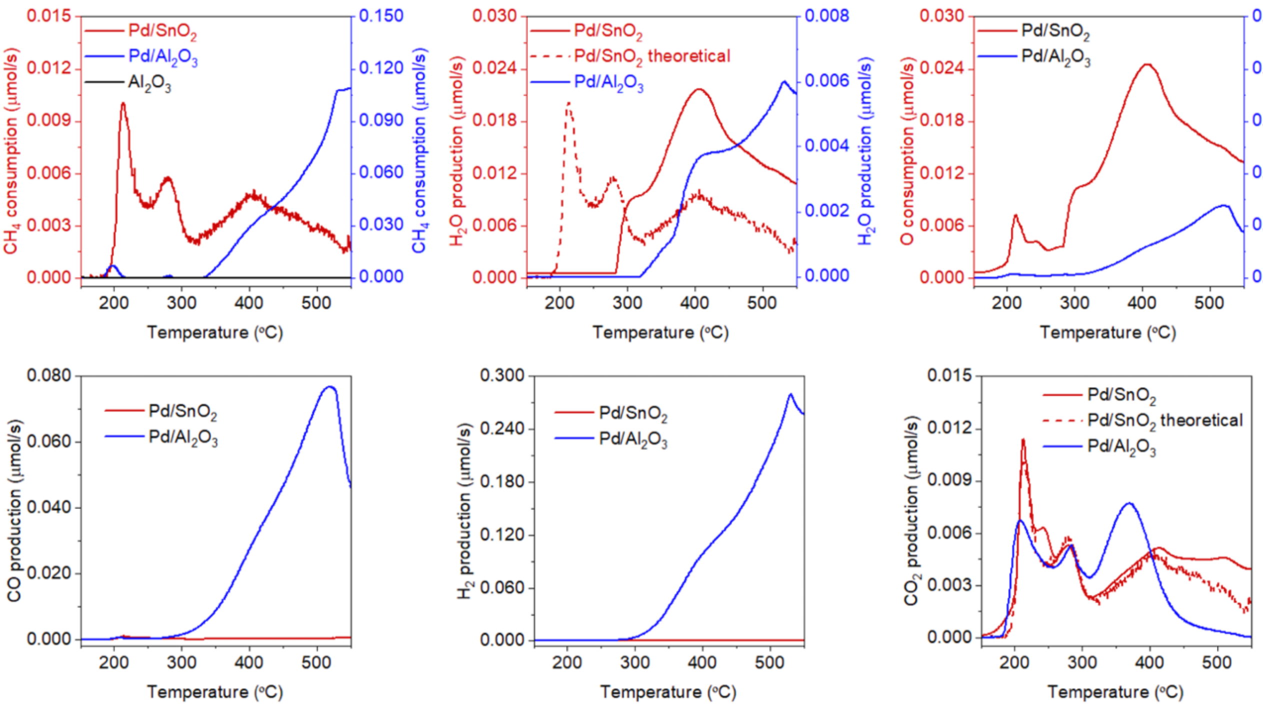

Figure 8. TPSR with CH_4 at anaerobic conditions at 5 °/min heating rate; 0.5 g of the calcined samples. Solid lines are experimental data measured by calibrated mass spectrometer; dash lines are theoretical data calculated using CH_4 consumption (for complete oxidation of CH_4).

The TPSRs in Figure 8 showed the same product distributions as was found in low-O_2 reactions (Figure 7): Pd/Al_2O_3 was able to convert methane to CO, H_2 and H_2O while Pd/SnO_2 did not produce any of CO and H_2. Water evolution on Pd/Al_2O_3 was concomitant with the onset of methane conversion, and some water was used for steam reforming. The Pd/SnO_2 catalyst also converted some CH_4 but only to CO_2. As seen by comparing the theoretical and experimental water release, H_2O release was significantly delayed on the Pd/SnO_2 catalyst, but when it started, all water was released from the catalyst, without converting to CO and H_2O. This again confirms that Pd/SnO_2 catalyst can retain water on SnO_2 and prevent its activation on Pd.

Based on the mass balance of exiting CO, H_2O and CO_2, we were able to calculate the amount of consumed catalyst-originated oxygen. For both catalysts it matched the Pd molar amount indicating that it was the oxygen stored in the catalyst as PdO. Neither Al_2O_3, nor SnO_2 donated any appreciative amount of lattice oxygen under the conditions studied. Temperature-programmed desorption of O_2 under He flow performed up to 1100 °C (Figure 9) demonstrated peaks only for the PdO/Pd transition. Only minor peaks were observed for SnO_2: the low temperature oxygen desorption peak centered at 610 °C can be ascribed to surface adsorbed O^- or O^{2-} species; while the high temperature peaks spanning from 700 – 1100 °C are the dissociation of lattice oxygen on SnO_2 surface.[52,53] The total area under the peaks for SnO_2 corresponds only to 0.04% of oxygen present in SnO_2. This finding is in line with metal-oxygen dissociation energy, which is 512 kJ/mol for Al-O (at 298K), 548 kJ/mol for Sn-O and 234 kJ/mol for Pd-O.[54] It is thus unlikely that SnO_2 donates its lattice oxygen to Pd, which explains that the amount of oxygen consumed for CH_4 conversion under anaerobic conditions matches the PdO content in the Pd/SnO_2 catalyst.

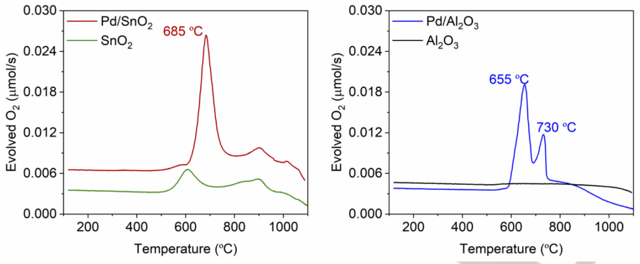

Figure 9. Oxygen desorption in He flow at 5 °/min heating rate. 0.5 g of the calcined samples.

Conclusions

- *In situ* temperature-programmed XAS of reduced Pd/Al_2O_3 catalyst during methane combustion in the wet feed with excess oxygen revealed that the major Pd(0) oxidation product was $Pd(OH)_2$ with minor amounts of PdO appearing at 350 °C. The dehydroxylation occurred above 450 °C.

- The reduced Pd/SnO_2 catalyst oxidized mainly to PdO, with significantly lower contributions from $Pd(OH)_2$ as compared to Pd/Al_2O_3. This explains the known higher water tolerance of the tin system in methane combustion.

- A variety of temperature-programmed reactions in low O_2 environment showed the striking feature of Pd/SnO_2 system of its inability to catalyze methane steam reforming, as opposed to Pd/Al_2O_3. The simplified bulk thermodynamic analysis of Pd, Sn and Al hydroxides dehydroxylation suggests that tin oxide can serve as a sink for hydroxyls extracted from $Pd(OH)_2$, while $Al(OH)_3$ can provide hydroxyls to Pd.

- The study suggests that supports with more favourable dehydroxylation ability than $Pd(OH)_2$ are able to extract poisonous hydroxyls from Pd/PdO particles and increase their activity in the wet methane combustion but decrease the methane steam reforming function.

- SnO_2-supported Pd catalysts are recommended for a follow-up investigation in a simulated multicomponent exhaust from natural-gas fuelled engines to evaluate their performance for potential commercialization. Melting points of SnO_2 and SnO (1, 630°C and 1,080°C, respectively) restrict their possible use to fuel-lean operations.

Experimental Section

Catalyst synthesis and pretreatment

The Pd/Al_2O_3 and Pd/SnO_2 catalysts were synthesized from preformed Pd nanoparticles deposited on commercial γ-Al_2O_3 (particle size 150 mesh, average pore size 58 Å, surface area 155 m^2/g, Sigma Aldrich) and tin(IV) dioxide (SnO_2, particle size 325 mesh, 99.9%, Sigma Aldrich). The nanoparticles were synthesized from palladium(II) acetate (98%, Sigma Aldrich) via polyol method and stabilized by polyvinylpyrrolidone (PVP, MW 40 000, Sigma Aldrich), as described earlier.[13] The obtained powders were calcined in static air at 550 °C for 16 h.

In situ XAS

An *in situ* XAS cell was used at the Canadian Light Source (CLS). The cell allows measurements of materials through transmission and/or fluorescence measurements at different temperatures and in different gaseous environments using both hard and soft X-Rays. The cell description can be found in the Supporting Information (Figure S2). At the beginning of the XAS experiment the samples were reduced by heating to 300 °C under a flow of 5% H_2 in N_2 for 10 minutes. The system was then cooled to 100 °C at which point the gaseous environment was changed to methane/air mixtures for the *in situ* experiment. 0.1% CH_4/N_2 and dry air were used at flow rates of 154 and 103 mL/min respectively, the dry air flowed through two bubblers to saturate it before mixing with the methane mix.[34] Temperature intervals generally started at 100 °C and were increased by 50 °C until 450 °C. The ramping rate was 10 °C/min, and once at the respective temperature the system was allowed to equilibrate for 10 minutes before measurements.

The Pd L edge and K edge spectra were collected at the Canadian Light Source on the Soft X-ray Microcharacterization Beamline (SXRMB) beamline and the Hard X-ray Microanalysis (HXMA) beamline, respectively, while Sn L edge data was collected on the SXRMB beamline. In the case of L edge data, the system was flushed with He immediately before the measurements were taken to reduce scattering on the incident and fluorescing photons (and the *in situ* conditions were resumed immediately after data collection). After normalization and energy calibration of the data, the data were analyzed by linear combination fitting (LCF) using IFEFFIT in the Demeter software package (Athena).[55] Three species were used as references for fitting: reduced Pd on metal oxide, fully oxidized PdO on metal oxide, and Pearlman's Catalyst $Pd(OH)_2/C$

(Sigma, 20 wt.%), metal oxide referring to SnO_2 or Al_2O_3 depending on the species being fit. The fit boundaries were set from -15 to +40 eV in the X-Ray Absorption Near Edge Structure (XANES) region of the XAS spectra.

For the *in situ* XAS studies the samples were 0.3 wt.% Pd/Al_2O_3 with 40% Pd dispersion and 0.2 wt.% Pd/SnO_2 with 16% Pd dispersion. The metal loadings were determined by neutron activation analysis and CO chemisorption (1:1 CO:Pd stoichiometry) as described earlier [13].

X-ray photoelectron spectroscopy (XPS)

XPS was performed using a Kratos AXIS Supra system. A 500 mm Rowland circle monochromated Al K-α (1486.6 eV) source was utilized in tandem with a hemi-spherical analyzer and spherical mirror analyzer. A 300x700 micron spot size was used. High resolution scans utilized 0.05 eV step sizes with a pass energy of 20 eV. Accelerating voltage was 15 keV with an emission current of 15 mA. XPS calibration was performed on adventitious carbon 1s peaks aligning carbon-carbon bonding to 284.8 eV.

Methane combustion at substoichiometric O_2/CH_4 ratios

All gas mixtures in this work were ordered from Praxair. Low-oxygen methane combustion tests were carried out in a AutoChem 2950 HP (Micromeritics) with an on-line mass spectrometer for product analysis (Pfeiffer Vacuum Thermostar GSD 320). The tested samples contained 0.4 wt% Pd each (confirmed by neutron activation analysis at Bureau Veritas, Canada). The metal dispersions measured by CO chemisorption on the same instruments before and after the catalytic tests were 9% (before) and 5% (after) for $Pd/\gamma\text{-}Al_2O_3$ and 8% (before) and 5% (after) for Pd/SnO_2. Prior to the dispersion measurements, the catalysts were reduced at 150 °C in H_2/He, followed by CO pulse adsorption and calcination in O_2/He at 550 °C for 1 h.

The catalytic tests were performed by temperature increase from 200 to 550 °C on the oxidized samples, 0.5 g each, 50 °C each step, 10 °C/min ramping rate, followed by cool down. Table 1 shows the test order and reaction mixture compositions. The mass spectrometer was calibrated for oxygen (32 m/z), methane (15 m/z), water (18 m/z), carbon monoxide (28 m/z) and carbon dioxide (44 m/z), hydrogen (2 m/z) and helium as an internal standard (4 m/z) prior to each test. Mass balance for He-exclusive components was above 92% in all tests. Every test was performed five times in each set, and two sets of tests were performed in variable methane concentration order. All tests systematically show less than 3% conversion deviation.

Table 1. Low-oxygen methane combustion test order. The flow rate of 1% O_2/He was constant at 120 mL/min

Test order	1	2	3	4	5
O_2/CH_4, mol/mol	1.3	1.9	1.0	1.5	1.1
10% CH_4/He, mL/min	9.3	6.3	12.2	7.8	10.7

Temperature-programmed surface reactions (TPSR) at anaerobic conditions were also performed with 0.5 g samples. After *in situ* calcination (10% O_2/He at 550 °C) the samples were cooled to 120 °C, followed by purging with He until no physisorbed oxygen was detected by the mass spectrometer. The reactions were carried out in 1.5% CH_4/He (23.5 mL/min) between 120 and 550 °C at a 5 °C/min heating rate. The amount of donated oxygen was calculated from mass balance of downstream CO, ½ CO_2 and H_2O.

Temperature-programmed reduction (TPR) and oxygen desorption

The TPR was performed with the same Autochem unit; hydrogen consumption was monitored by the calibrated mass spectrometer. 0.5 g of the calcined catalysts were pretreated in situ by reduction and oxidation at 550 °C. The TPR analyses were performed in 5% H_2/He, 20 mL/min, up to 550 °C with a ramping rate of 10 °C/min.

The temperature-programmed oxygen desorption (TPD) was also done with 0.5 g catalysts with the same setup. The samples were calcined in 10% O_2/He at 1100 °C for 10 min, cooled down to 120 °C and flushed with He to remove physisorbed O_2. The TPD analyses were carried out up with a heating rate of 5 °C/min in He (50 mL/min), the concentration of evolved O_2 was quantified by the mass spectrometer.

Acknowledgements

We thank Dr. Danielle Covelli at the University of Saskatchewan's Saskatchewan Structural Sciences Centre (SSSC) for assistance with XPS acquisition. We thank Dr. Hanieh Nassiri (Univeristy of Alberta) for the data in Figure 1, and Dr. Ning Chen and Weifeng Chen on the HXMA beamline for assistance with high energy XAS measurements. The XAS work was performed at the Canadian Light Source, which is supported by the Canadian Foundation for Innovation, Natural Sciences and Engineering Research Council of Canada, the University of Saskatchewan, the Government of Saskatchewan, Western Economic Diversification Canada, the National Research Council Canada, and the Canadian Institutes of Health Research. Financial support from Natural Sciences and Engineering Research Council of Canada (NSERC Strategic grant STPGP 478979-15) is appreciated.

Keywords: heterogeneous catalysis • methane combustion • tin oxide • palladium • X-ray absorption spectroscopy

[1] W. Huang, E. D. Goodman, P. Losch, M. Cargnello, *Ind. Eng. Chem. Res.* **2018**, *57*, 10261.
[2] R. Burch, F. J. Urbano, P. K. Loader, *Appl. Catal. A, Gen.* **1995**, *123*, 173.
[3] P. Losch, W. Huang, O. Vozniuk, E. D. Goodman, W. Schmidt, M. Cargnello, *ACS Catal.* **2019**, 4742.
[4] D. Ciuparu, E. Perkins, L. Pfefferle, *Appl. Catal. A Gen.* **2004**, *263*, 145.
[5] D. Ciuparu, L. Pfefferle, *Appl. Catal. A Gen.* **2001**, *209*, 415.
[6] W. R. Schwartz, L. D. Pfefferle, *J. Phys. Chem. C* **2012**, *116*, 8571.
[7] W. R. Schwartz, D. Ciuparu, L. D. Pfefferle, *J. Phys. Chem. C* **2012**, *116*, 8587.
[8] M. Monai, T. Montini, C. Chen, E. Fonda, R. J. Gorte, P. Fornasiero, *ChemCatChem* **2015**, *7*, 2038.
[9] H. Nassiri, K.-E. Lee, Y. Hu, R. E. Hayes, R. W. J. Scott, N. Semagina, *J. Catal.* **2017**, *352*, 649.
[10] P. Lott, P. Dolcet, M. Casapu, J.-D. Grunwaldt, O. Deutschmann, *Ind. Eng. Chem. Res.* **2019**, *58*, 12561.
[11] R. Kikuchi, S. Maeda, K. Sasaki, S. Wennerström, K. Eguchi, *Appl. Catal. A Gen.* **2002**, *232*, 23.
[12] J. Yu, D. Zhao, X. Xu, X. Wang, N. Zhang, *ChemCatChem* **2012**, *4*, 1122.
[13] H. Nassiri, R. E. Hayes, N. Semagina, *Top. Catal.* **2019**, *62*, 386.

[14] Z. Zhao, B. Wang, J. Ma, W. Zhan, L. Wang, Y. Y. Guo, Y. Y. Guo, G. Lu, *Cuihua Xuebao/Chinese J. Catal.* **2017**, *38*, 1322.

[15] S. A. Müller, D. Degler, C. Feldmann, M. Türk, R. Moos, K. Fink, F. Studt, D. Gerthsen, N. Bârsan, J. D. Grunwaldt, *ChemCatChem* **2018**, *10*, 864.

[16] G. Croft, M. J. Fuller, *Nature* **1977**, *269*, 585.

[17] T. Itoh, I. Matsubara, M. Kadosaki, Y. Sakai, W. Shin, N. Izu, M. Nishibori, *Sensors* **2010**, *10*, 6513.

[18] S. Wicker, M. Guiltat, U. Weimar, A. Hémeryck, N. Barsan, *J. Phys. Chem. C* **2017**, *121*, 25064.

[19] S. H. Hahn, N. Bârsan, U. Weimar, S. G. Ejakov, J. H. Visser, R. E. Soltis, *Thin Solid Films* **2003**, *436*, 17.

[20] D. Koziej, N. Bârsan, U. Weimar, J. Szuber, K. Shimanoe, N. Yamazoe, *Chem. Phys. Lett.* **2005**, *410*, 321.

[21] M. Hübner, R. G. Pavelko, N. Barsan, U. Weimar, *Sens. Actuators, B Chem.* **2011**, *154*, 264.

[22] J. Miao, C. Chen, Y. S. Lin, *J. Phys. Chem. C* **2018**, *122*, 21322.

[23] A. Marikutsa, M. Rumyantseva, A. Gaskov, *J. Phys. Chem. C* **2015**, *119*, 24342.

[24] E. Ogel, S. A. Müller, A. Sackmann, F. Gyger, P. Bockstaller, E. Brose, M. Casapu, L. Schöttner, D. Gerthsen, C. Feldmann, J.-D. Grunwaldt, *ChemCatChem* **2017**, *9*, 407.

[25] P. G. Harrison, M. J. Willett, *Nature* **1988**, *332*, 337.

[26] N. Barsan, U. Weimar, *J. Phys. Condens. Matter* **2003**, *15*, 813.

[27] J. Tamaki, M. Nasaishi, Y. Teraola, N. Miura, N. Yamazoe, K. Moriya, Y. Nakamura, *Surf. Sci.* **1989**, *221*, 183.

[28] J. C. Kim, H. K. Jun, J. S. Huh, D. D. Lee, *Sens. Actuators B Chem.* **1997**, *45*, 271.

[29] G. Tournier, C. Pijolat, *Sens. Actuators B Chem.* **1999**, *61*, 43.

[30] S. Emiroglu, N. Bârsan, U. Weimar, V. Hoffmann, *Thin Solid Films* **2001**, *391*, 176.

[31] D. Haridas, V. Gupta, *Sens. Actuators B Chem.* **2012**, *166–167*, 156.

[32] K. Grossmann, R. G. Pavelko, N. Barsan, U. Weimar, *Sens. Actuators B Chem.* **2012**, *166–167*, 787.

[33] G. Yang, A. I. Frenkel, D. Su, X. Teng, *ChemCatChem* **2016**, *8*, 2876.

[34] H. Nassiri, K.-E. Lee, Y. Hu, R. E. Hayes, R. W. J. Scott, N. Semagina, *ChemPhysChem* **2017**, *18*, 238.

[35] Y. Mahara, K. Murata, K. Ueda, J. Ohyama, K. Kato, A. Satsuma, *ChemCatChem* **2018**, *10*, 3384.

[36] A. Auroux, D. Sprinceana, A. Gervasini, *J. Catal.* **2000**, *195*, 140.

[37] H. Yamaura, S. Hirao, S. Yamaguchi, H. Yahiro, *Sensors Mater.* **2017**, *28*, 1203.

[38] S. Chai, X. Bai, J. Li, C. Liu, T. Ding, Y. Tian, C. Liu, H. Xian, W. Mi, X. Li, *Appl. Surf. Sci.* **2017**, *402*, 12.

[39] P. W. Albers, K. Möbus, S. D. Wieland, S. F. Parker, *Phys. Chem. Chem. Phys.* **2015**, *17*, 5274.

[40] H. Stotz, L. Maier, A. Boubnov, A. T. Gremminger, J. D. Grunwaldt, O. Deutschmann, *J. Catal.* **2019**, *370*, 152.

[41] E. D. Goodman, A. A. Ye, A. Aitbekova, O. Mueller, A. R. Riscoe, T. N. Taylor, A. S. Hoffman, A. Boubnov, K. C. Bustillo, M. Nachtegaal, S. R. Bare, M. Cargnello, *J. Chem. Phys.* **2019**, *151*, 154703.

[42] J. J. Willis, A. Gallo, D. Sokaras, H. Aljama, S. H. Nowak, E. D. Goodman, L. Wu, C. J. Tassone, T. F. Jaramillo, F. Abild-Pedersen, M. Cargnello, *ACS Catal.* **2017**, *7*, 7810.

[43] Y.-H. Chin, M. Garcia-Dieguez, E. Iglesia, *J. Phys. Chem. C* **2016**, *120*, 1446.

[44] H. Xiong, K. Lester, T. Ressler, R. Schlogl, L. F. Allardm A. K. Datye, *Catal. Lett.* **2017**, *147*, 1095.

[45] G. Verdes, R. Gout, S. Castet, *Eur. J. Mineral.* **2014**, *4*, 767.

[46] D. Wagman, W. Evans, V. Parker, R. Schumm, I. Halow, S. Bailey, K. Churney, R. Nuttal, *J. Phys. Chem. Ref. Data* **1982**, *11*, 1.

[47] N. N. Smirnova, T. A. Bykova, N. A. Polotnyanko, N. D. Shikina, I. L. Khodakovskii, *Russ. J. Phys. Chem. A* **2010**, *84*, 1851.

[48] C. F. Cullis, T. G. Nevell, D. L. Trimm, *J. Chem. Soc. Faraday Trans. 1 Phys. Chem. Condens. Phases* **1972**, *68*, 1406.

[49] N. Mouaddib, C. Feumi-Jantou, E. Garbowski, M. Primet, *Appl. Catal. A, Gen.* **1992**, *87*, 129.

[50] J. J. Willis, E. D. Goodman, L. Wu, A. R. Riscoe, P. Martins, C. J. Tassone, M. Cargnello, *J. Am. Chem. Soc.* **2017**, *139*, 11989.

[51] H. Wang, Z. Liu, Y. Ma, K. Julian, S. Ji, V. Linkov, R. Wang, *Phys. Chem. Chem. Phys.* **2013**, *15*, 13999.

[52] F. Gaillard, J.-P. Joly, A. Perrard, *Adsorpt. Sci. Technol.* **2008**, *25*, 245.

[53] N. Yamazoe, J. Fuchigami, M. Kishikawa, T. Seiyama, *Surf. Sci.* **1979**, *86*, 335.

[54] Y.-R. Luo in *CRC Handbook of Chemistry and Physics* (Ed.: W.M. Haynes), CRC Press Taylor & Francis Group, Boca Raton, London, New York, **2012**, pp. 9–65.

[55] B. Ravel, M. Newville, *J. Synchrotron Radiat.* **2005**, *12*, 537.

Entry for the Table of Contents

FULL PAPER

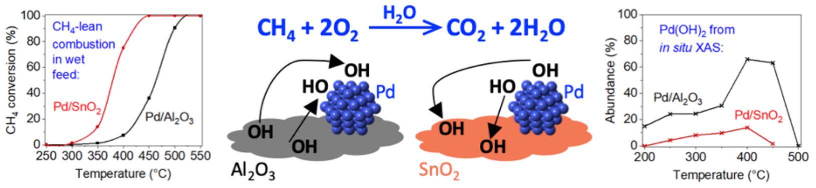

Hydroxyls away! Tin oxide extracts hydroxyls from Pd and liberates it for methane combustion but renders Pd inactive for methane steam reforming, as opposed to Pd/Al_2O_3. Quantitative analysis of metallic Pd, PdO, and Pd$(OH)_2$ is presented for Pd/Al_2O_3 and Pd/SnO_2 catalysts as a function of temperature during methane-lean combustion in the presence of water, as found by in situ X-ray absorption spectroscopy.

William Barrett, Jing Shen, Yongfeng Hu, Robert E. Hayes, Robert W.J. Scott, Natalia Semagina**

Page No. – Page No.

Understanding the role of SnO_2 support in water-tolerant methane combustion: *In situ* observation of Pd$(OH)_2$ and comparison with Pd/Al_2O_3